Ab Initio Molecular Dynamics Simulation of Water Transport through Short Carbon Nanotubes

Dongfei Liu, Jipeng Li, Jianzhong Wu, and Diannan Lu*

ACCESS | Metrics & More | Article Recommendations | SI Supporting Information

ABSTRACT: Water transport through short single-walled (6, 6) carbon nanotubes (CNTs) was investigated with *ab initio* molecular dynamics (AIMD) simulation at different temperatures. The water molecules under extreme confinement present a one-dimensional jagged pattern owing to hydrogen bonding, with the near-perfect alignment of the dipole orientations. CNTs ending with dangling bonds can promote water dissociation near the entrance and the occurrence of dipole flipping along the water wire at high temperatures, accompanied by the formation of D defects and L defects in the hydrogen-bond network. In contrast, dissociation of water molecules rarely takes place if the dangling bonds at the ends of the CNTs are terminated with H atoms. Angular jumps of water molecules are commonplace inside the narrow CNTs, implying a low-energy barrier for hydrogen-bond exchange among water molecules in narrow CNTs. The simulation results demonstrate the high activity of dangling bonds at the ends of short CNTs, accompanying passivation processes and their profound impact on water structure and transport, which is important for diverse technological applications.
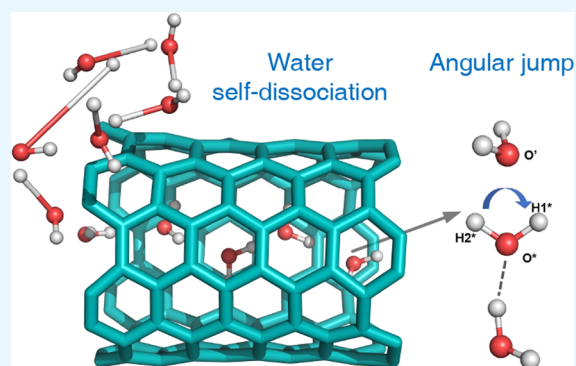
INTRODUCTION

Liquid water under nanoscale confinement is drastically different from that in the bulk phase, especially in terms of the hydrogen-bond network, transport behavior, and chemical reactivity.[1−3] The unique properties of water molecules under extreme confinement have inspired the design of artificial nanochannels or nanopores to address a wide array of technological challenges in water desalination,[4−7] biosensing,[8,9] energy conversion,[10] and nanofluidic logic and gating.[11] Among diverse nanostructured materials that can be utilized to regulate water structure and transport at molecular scales, carbon nanotubes (CNTs) provide a simple platform for studying the unique behaviors of water molecules in confinement because the nanopores can be controlled with atomic precision and advanced functionalization methods are available to manipulate both the entrance and the surface properties.[12,13] Furthermore, the dimensions of narrow CNTs are comparable to those of water and ion channels in biological systems, and they are widely used as biomimetic channels.[14] For example, biomimetic nanopores based on membrane-spanning single-walled CNTs have been designed to include selectivity filters based on combinations of anionic and cationic groups.[15] One may develop CNT porins that self-insert into lipid bilayers to mimic aquaporin channel functionality and intrachannel single-file water arrangement.[16]

A large number of experimental and computational research studies have been devoted to examining the structure and dynamic properties of water in CNTs.[1,17−28] Koga et al. carried out classical molecular dynamics (MD) simulations on the phase behavior of water in CNTs and predicted a continuous transformation of liquid water into new ice phases at high axial pressures.[2] A regular water structure, *i.e.*, a one-dimensional chain of water molecules was also predicted by MD simulations inside narrow (6, 6) CNTs (with an inner diameter of 0.81 nm).[1] Water molecules in larger CNTs exhibit a layered structure with spiraling strands along the CNT axis.[2,20] Brewer et al. predicted that the proton transport rate in narrow channels was 10 times higher than that in bulk water using the multistate empirical valence bond (MS-EVB) model.[29] Various mechanisms have been proposed to explain the ultrafast transport of protons under nanoconfinement, including vehicular diffusion,[30] Grotthuss diffusion,[31] and Zundel−Zundel transition.[32] In addition, the dynamic behaviors of water molecules inside CNTs have also attracted significant interest. Berezhkovskii et al. proposed a continuous-time random-walk (CTRW) model to describe the proton transport behavior through nanochannels densely filled with water molecules in a single-file arrangement.[33] Majumder et al.
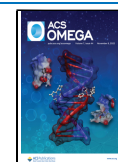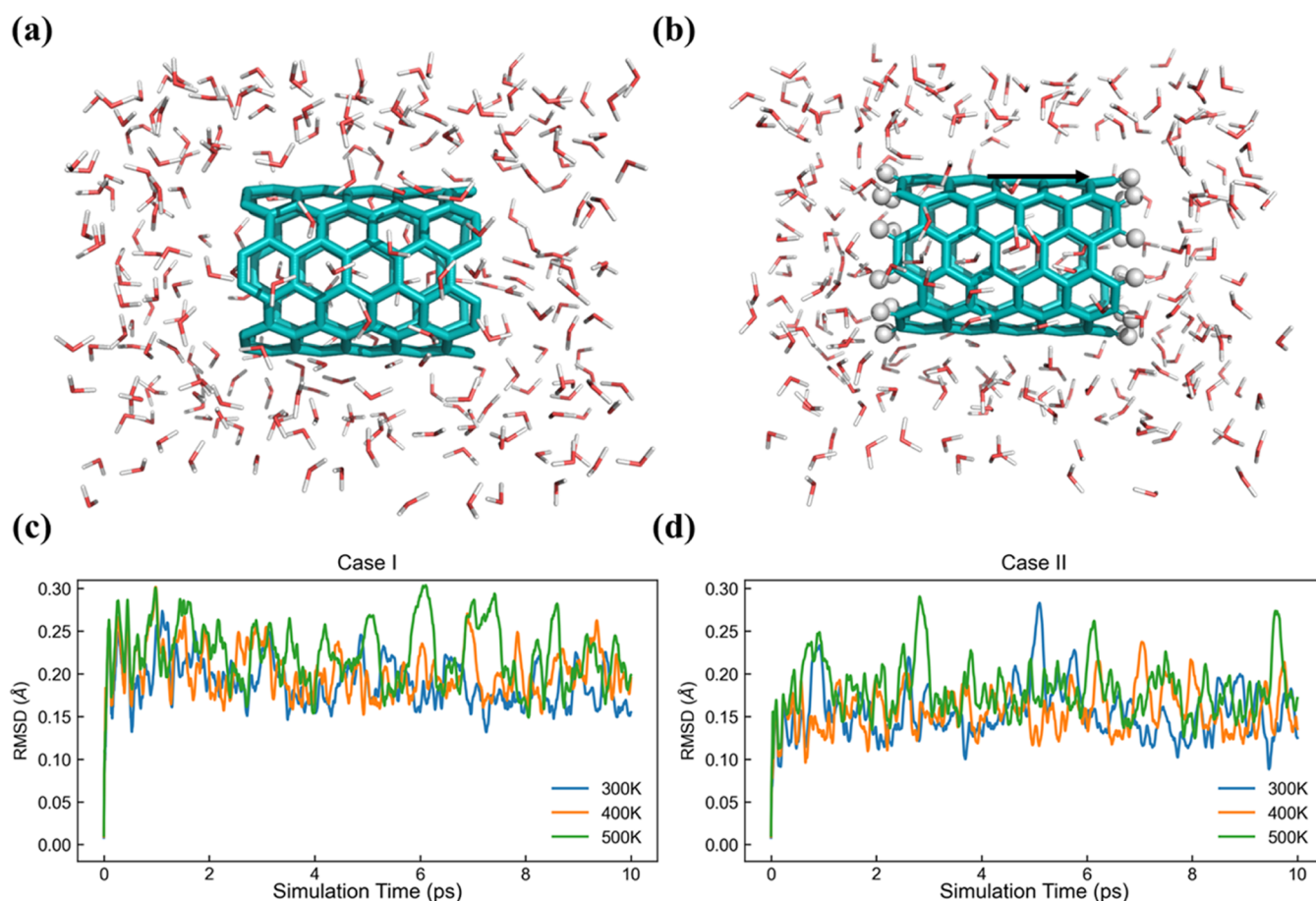
Figure 1. Narrow CNTs in liquid water with dangling bonds at the ends, Case I (a) or with the ends capped by hydrogen atoms, Case II (b). Fluctuation of the CNT structure is measured in terms of the root-mean-square deviation (RMSD) from the initial configuration of CNTs in Case I (c) and Case II (d) at 300, 400, and 500 K.

reported that liquid water flows through a CNT array faster than that predicted by the Hagen−Poiseuille theory by 4−5 orders of magnitude.[18] MD simulations by Falk et al. corroborated the flow enhancement, on the order of 10^3 to 10^4 for CNTs with a diameter in the range of 1−2 nm and 10 for those with a diameter of about 50 nm.[34] The simulation results were consistent with the experimental measurements under similar conditions.[35] Lu investigated water transport through charged CNTs and found that the surface charge has strong effects on hydrogen bonding between water molecules inside the nanotubes and on the bipolar properties of water chains.[36] Liu et al. explored the influence of the helicity of CNTs on the diffusion of confined water and found that water molecules diffuse in zigzag CNTs much slower than in armchair CNTs due to the higher activation energy.[37] The results were supported by Sam and Sathian who also found that the effect of helicity or chirality of CNTs on water transport decreases with increasing the nanotube diameter.[24]

Although computational studies have played an important role in understanding the atomistic structure and dynamic behavior of water in CNTs, most classical water models are calibrated with bulk properties of liquid water that may not accurately describe the confinement effects. In addition, different water models often present discrepancies in MD simulation. For example, Losey et al. tested various atomistic models of water for studying the flux through CNTs and found that the results were strongly dependent on the models used in

the MD simulation.[25] The classical models of water molecules, such as simple-point-charge (SPC),[38] extended simple-point-charge (SPC/E),[39] and TIP3P,[40] assume a rigid structure with both the bond length and bond angle fixed in the simulation. The rigidity is not conducive to the dynamic characteristics of hydrogen bonding in the system. In contrast, *ab initio* MD (AIMD)[41,42] simulation is able to calculate the atomic forces on the fly and captures bond formation and breakage as naturally taking place in liquid water. Due to the computational cost, there have been only a few studies using AIMD to investigate the microscopic structure and dynamic behavior of water molecules in CNTs.[43,44] A recent study[45] has explored water flow in CNTs using a machine learning potential approach, which maintains the accuracy of AIMD and circumvents its high computational cost. However, this study tried to make enough water inside the CNTs so as to approach the bulk water state, different from the system with single-file water inside the CNTs. Furthermore, these previous studies mostly focused on water molecules in the infinitely long CNTs, which have periodic boundaries along the axis. That is to say, there are no so-called water molecules entering or leaving the CNTs. Actually, the issue of entrance effects is particularly important for channels with a nanoscale and there is a fundamental dissipation arising from the connection between the channel and the bulk water.[46]

In this work, we have carried out AIMD simulations to investigate the structure and dynamic behaviors of water
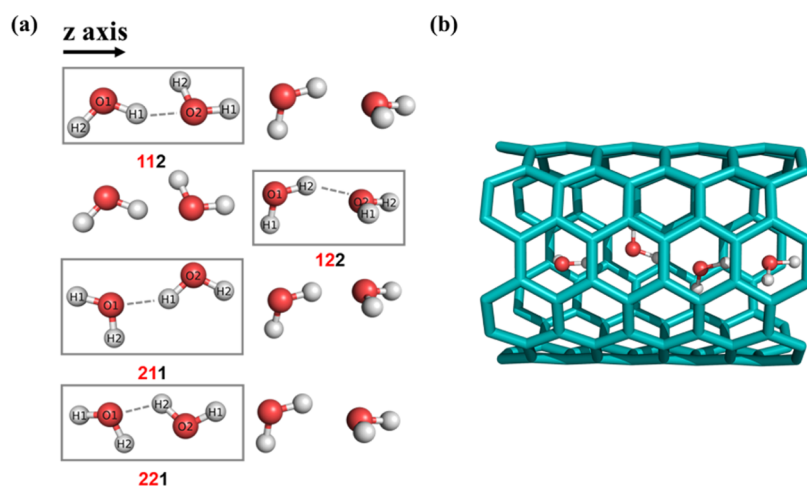
Figure 2. (a) Four types of hydrogen bonds between water molecules in narrow CNTs. (b) Water molecules inside the CNTs form a jagged pattern.

molecules in short armchair CNTs immersed in liquid water. Two types of CNT models were used in our AIMD simulation: one with dangling bonds at the two ends of the CNTs (Case I, Figure 1a), and the other with these dangling bonds capped with H atoms (Case II, Figure 1b). For both CNT models, we performed AIMD simulations at three temperatures (300, 400, and 500 K) to investigate the thermal fluctuation effects. The simulation results allow us to evaluate the number of water molecules entering the CNT pore, the linearity of their arrangements inside the nanopore, and the relative orientations of water dipoles. In addition, we studied the angular jump of hydrogen bonds in the one-dimensional water chain and the dipole flip inside the CNTs at different temperatures. Special attention was paid to the terminal effects on the orientational defects of the water chains formed inside the CNTs. We found that the dangling bonds from the CNTs' ends led to the irreversible dissociation of water molecules and promoted proton transportation outside the nanopore. As the water molecules dissociated, the products would quickly passivate the C atoms with dangling bonds. The simulation results highlight the importance of dangling bonds and confinement effects on the water structure and transport through narrow CNTs.

MODEL SYSTEM AND COMPUTATIONAL METHODS

Model System. Our model system consists of 11 Å long (6, 6) single-walled CNTs immersed in bulk water. The simulation box has the dimensions of $20 \times 20 \times 26$ Å^3. The narrow CNTs are made of 120 carbon atoms with dangling bonds at the ends or with the ends of the CNTs capped with 24 hydrogen atoms. In Case I, the CNTs are solvated with 253 water molecules, and thus the simulation cell contains a total of 879 atoms. In Case II, the CNTs are surrounded by 249 water molecules, and the total number of atoms simulated is 891. Figure 1a,b shows snapshots of Case I and Case II, respectively, with the CNTs placed at the center of the simulation cell.

Simulation Methods. The simulation protocol is the same for both cases. Before the AIMD simulation, the water molecules and CNT atoms were relaxed to reach an equilibrium configuration through classical MD simulation. Toward this end, we used the GROMACS program[47] with the water molecules represented by the extended simple-point-

charge (SPC/E) model and their interactions with the CNT atoms described by the GROMOS 54A7 force field.[48] The initial configuration of the water molecules for AIMD simulation was obtained through energy minimization and 100 ps canonical (NVT) ensemble classical MD simulation with a fixed CNT structure.

Next, AIMD simulations were conducted using the Quickstep program implemented in the *cp2k* package.[42,49] The electronic structures were calculated from the density functional theory (DFT) with the Perdew−Burke−Ernzerhof (PBE) functional[50] and the Goedecker−Teter−Hutter (GTH) pseudopotentials[51] for core electrons. Considering the large number of atoms in the simulation cell, we chose a simpler GTH double-ζ-valence-polarized (DZVP) Gaussian basis in combination with a plane-wave basis set for AIMD simulations. The energy cutoff was 280 Ry.[52] The van der Waals (vdW) dispersion correction was considered to account for the weak interaction among water molecules.[53] For both cases, the AIMD simulations were carried out in a canonical (NVT) ensemble at three temperatures (300, 400, and 500 K). The periodic boundary conditions were imposed in all directions. Owing to the high computational cost, AIMD simulations were performed for 10 ps with a time step of 1 fs. It is worth noting that we did not fix the CNT structure in the simulation, which was more in line with the actual scenario. Some differences were noticeable between the initial and the final structures of the CNTs after AIMD simulations. The root-mean-square deviation (RMSD) of atomic positions was around 0.21 Å for the CNTs with dangling bonds (Case I) and 0.16 Å for the CNTs ending with hydrogen carbons (Case II). Figure 1c,d compares the variations of RMSD with the simulation time for two cases at different temperatures. To a certain degree, the variations in RMSD also reflect the thermal fluctuations of carbon atoms, *i.e.*, the higher the temperature, the more drastic the fluctuations.

Analysis. To analyze the hydrogen bonds among water molecules inside the CNTs, we set the criteria for hydrogen bonding such that the distance between two oxygen atoms is less than 3.5 Å and the oxygen−hydrogen−oxygen bond angle is within 30°. In addition, we defined four types of hydrogen bonds for water molecules inside the CNTs, as shown in Figure 2a, numerically labeled with "112", "122", "211", and "221" according to the molecular origins of the participating
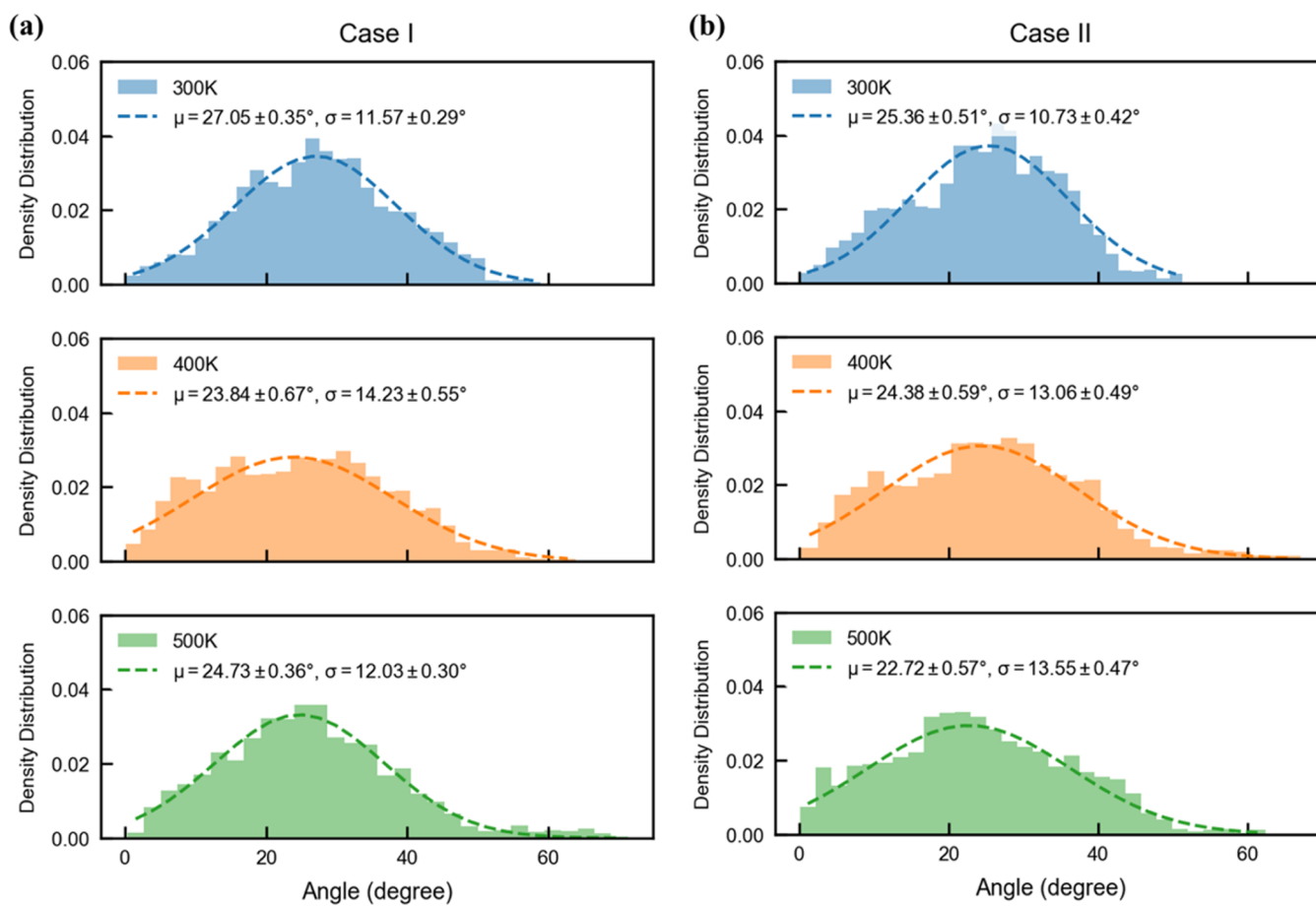
Figure 3. Probability density of the angles between the O_iO_{i+1} vectors and the axial direction is predicted by the AIMD simulation for Case I (a) and Case II (b) at 300, 400, and 500 K.

atoms in hydrogen bond formation. For hydrogen bonding between two neighboring water molecules within the CNTs, the 1st and 3rd positions in the string (*e.g.*, "112") refer to O atoms of the water molecules, and the characters "1" and "2" correspond to atoms closer or further away from a specified end of the CNTs. The number in the 2nd position of the string refers to the origin of the hydrogen connecting the oxygen atoms, *i.e.*, "1" means the hydrogen from the first water molecule and "2" from the second hydrogen of the first water molecule. The first two numbers in the string correspond to the proton donor water molecule, while the last number denotes the oxygen atoms of the proton acceptor water molecule.

■ RESULTS AND DISCUSSION

Water Molecules Inside the CNTs. As shown in previous studies, our AIMD simulation indicates that water molecules are arranged in a single-file structure in the narrow CNTs.[1,3,33] Figure S1a,b in the Supporting Information presents the evolution of the number of water molecules inside the CNTs for Case I and Case II at 300, 400, and 500 K. On average, there are about three to five water molecules entering the CNTs during the course of the simulation. Given that the length of the hydrogen bond, *i.e.*, the distance between the donor O atom and the acceptor O atom, is in the range between 2.2 and 3 Å, the water density in the CNTs is reasonable and consistent with that obtained from the previous simulation.[1,22,25,27] The spikes shown in Figure S1a,b arise

from the transient entry or exit of individual water molecules through the ends of the CNTs. Lowering the temperature promotes more water molecules entering the CNTs for both Cases I and II. The trend is understandable because the entropic effect due to water confinement becomes more prominent when temperature increases. While the length of CNTs is identical in Cases I and II, significant differences are observed in the average number of water molecules in the CNTs, especially at high temperatures. Fewer water molecules are observed inside the CNTs for Case II, in which the CNTs' ends are modified by H atoms. The reduction in water adsorption may be attributed to the steric resistance at the entrance or the hydrophobicity of hydrogen atoms at the two ends of the CNTs of Case II. Furthermore, the dangling bonds at the ends of CNTs in Case I are chemically reactive[54] and tend to attract other atoms to form covalent bonds, which is also commonly referred to as a passivation process. In the final part of this study, we will also discuss this problem in the context of passivation.

Jagged Water Molecule Chain Inside the CNTs. The results from AIMD simulation indicate that though water molecules inside the CNTs are aligned in a single-file structure, not all O atoms are distributed along the axis of the nanotube.[44] Instead, they are arranged in a jagged pattern regardless of the terminations (Figure 2b). Figure 3a,b shows the probability distributions of the angle between the O_iO_{i+1} vector and the axial direction predicted by the AIMD simulation for Cases I and II at 300, 400, and 500 K. Here
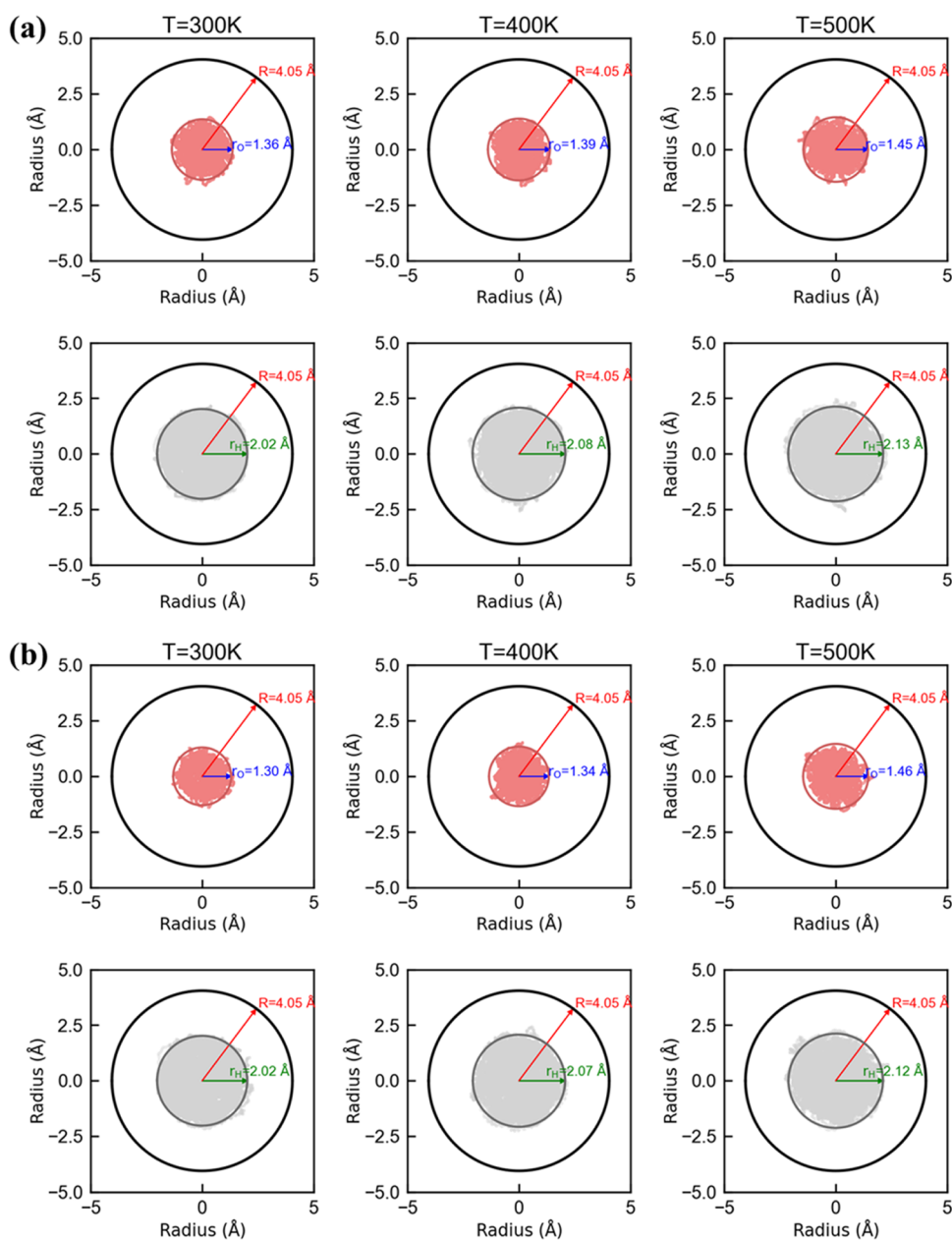
Figure 4. Projections of O and H atoms on the cross-sectional area of the CNTs in Case I (a) and Case II (b). The dots in the figures are projections of the atomic positions (red for oxygen atoms and gray for hydrogen atoms). The radii marked in the figures are the 99th percentile of all atomic positions (blue for oxygen atoms and green for hydrogen atoms).

the O_iO_{i+1} vector is determined by the two O atoms from adjacent water molecules confined in the CNTs. It can be seen from Figure 3a,b that the orientations of O_iO_{i+1} vectors approximately follow a normal distribution with an average of 25.2° for Case I and 24.5° for Case II relative to the axial direction (viz., z-axis). The angles between the O_iO_{i+1} vector and the z-axis in Case I are a little greater than that in Case II because it adsorbs more water molecules inside the CNTs. The orientational distribution of O_iO_{i+1} vectors is closely affiliated with the directional nature of hydrogen bonding among water molecules in the CNTs.

In addition to the positions of the oxygen atoms in the axial direction, we also analyzed the distributions of oxygen and hydrogen atoms in the radial direction. Figure 4a,b shows the projections of O and H atoms in the cross-sectional area of the CNTs for Case I and Case II, respectively. In both cases, the O

and H atoms are strongly localized near the center due to the hydrogen bonding among water molecules and the confinement of the nanotube wall. Although O atoms are not positioned exactly on the z-axis, their projections on the cross-sectional area of the CNTs are confined within a circular region of radius $r \approx 1.40$ Å. The H atoms are projected over a much larger circular region, with a radius of approximately $r \approx 2.08$ Å. For Case II, the projections of O atoms and H atoms are limited to circular regions of similar sizes compared to those for Case I. For both cases, the (maximum) radius increases slightly with temperature due to the entropic effects or thermal effects. Figure S2a,b gives the radial position distribution of O atoms and H atoms of Case I and Case II at different temperatures. As expected, the atomic distributions inside the nanotube are highly nonuniform in the radial direction. While the O atoms are concentrated in the region
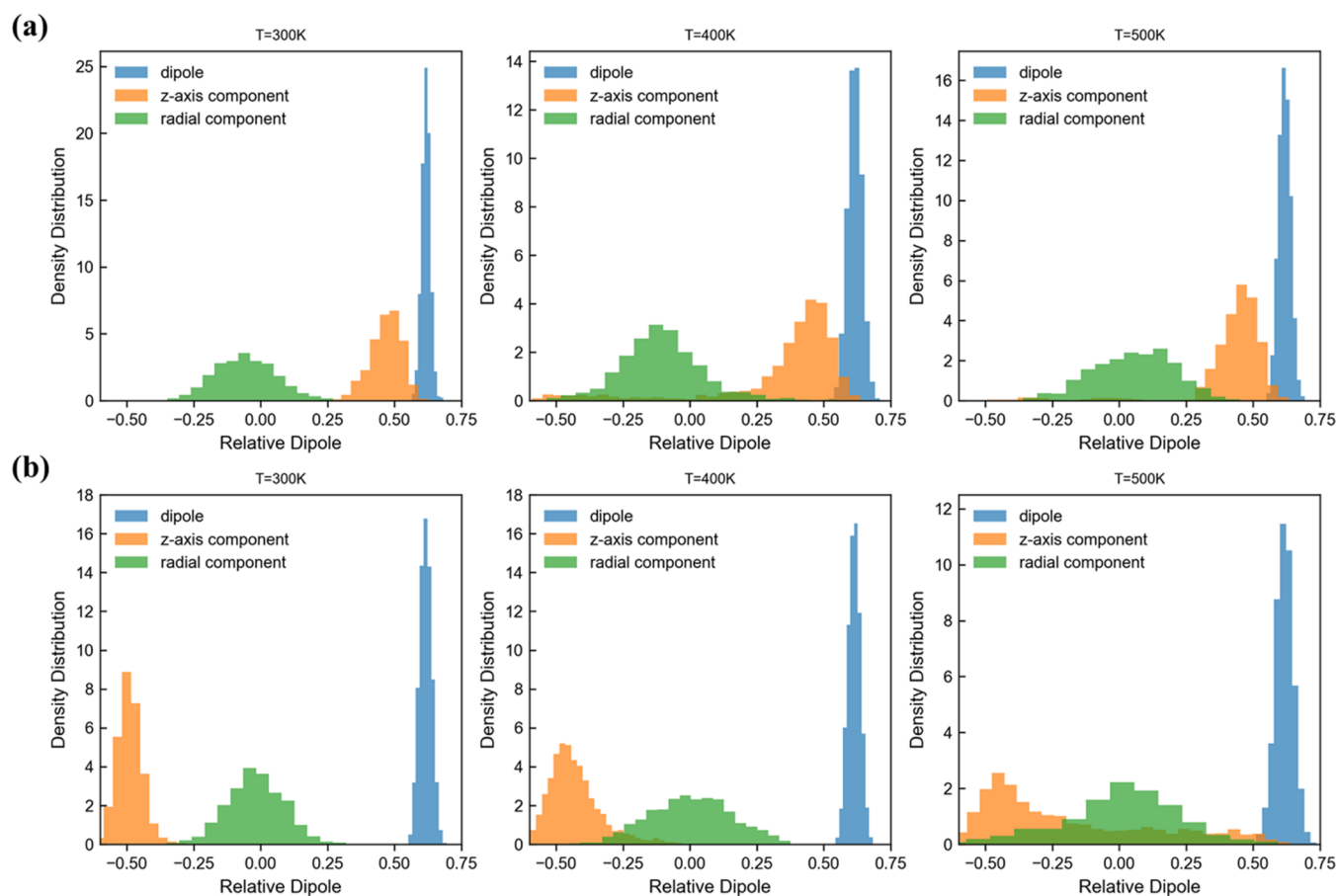
Figure 5. Statistical histograms for the relative dipole moments of water molecules in the CNTs with dangling bonds at the ends (a) and without dangling bonds (b). The axial (orange) and radial (green) components of the dipole reflect the orientations of confined water molecules.

around $r = 0.75$ Å, the H atoms are clustered in the area near $r = 0.25$ Å with a small peak at $r = 1.25$ Å at lower temperatures. These distribution characteristics indirectly manifest that the dipole of water molecules inside the CNTs is at a small acute angle to the z-axis and the water molecules inside the CNTs are aligned in a jagged chain, thus ensuring that H atoms are close to the axis. For Case II at 500 K, the radial position distribution of O atoms exhibits a peak position around $r = 0.5$ Å, much closer to the center compared to other temperatures. The stronger confinement effect may be attributed to the fewer water molecules inside the nanotube compared with Case I at 500 K and, consequently, fewer hydrogen bonds, only one or even zero. With less constraints from neighboring molecules, water molecules inside the CNTs tend to stay closer to the z-axis. Overall, the temperature effects on the radial position distributions of O and H atoms in Case I and Case II are relatively insignificant, which reflects the fact that the water structure inside the CNTs is primarily determined by hydrogen bonding and confinement. In addition, the dangling bonds at the ends of the CNTs have few influences on the radial movement of water molecules inside.

Relative Dipole Moments Distribution and Dipole Flip. The dipole moment is an important physical quantity that characterizes the polarity and orientation of any polar molecule. To explore how the confinement affects the dipole moment of water molecules inside the CNTs, we may calculate the partial charges of O and H atoms from the electronic structure. Because the procedure is model dependent, in the following, we consider only the relative dipole of each water

molecule, i.e., the dipole moment is calculated by assigning each O atom with 1 unit of negative charge or $-e$ and each H atom with half of the unit positive charge or $+0.5e$; e is the elementary charge. Then, the relative dipole μ_R can be written as $\mu_R = \sqrt{\mu_x^2 + \mu_y^2 + \mu_z^2}/e$ Å. μ_x is the x-component of the relative dipole moment, defined as $\mu_x = \sum_j q_j x_j$. Here, q_j is the partial charge of atom j, x_j is the x-coordinate of atom j, and the sum is over all of the atoms in the water molecule. Similar expressions are used for the y- and z- components. It can be seen that the relative dipole here is dimensionless.

Figure 4a,b shows the statistical histograms of the relative dipole moments of water molecules in the CNTs for Case I and Case II, respectively. Also shown in these figures are the axial and radial components of the dipoles calculated from AIMD. It can be seen that, at each temperature, the relative dipole moments and the corresponding axial and radial components approximately follow the normal distribution. The probability distribution for the total moments is significantly more concentrated than the distributions of the axial and radial components, which reflects the rigidity of the water molecules and the flexibility of molecular orientations. The magnitude of the relative dipole moment fluctuates slightly around 0.62. More importantly, the axial components of the relative dipole moment are distributed around 0.45 or −0.45, which is different from the radial components, which are distributed around 0.1 or −0.1, much smaller than the axial components. It is worth noting that the selected z-axis direction for Case II is opposite to that for Case I, not
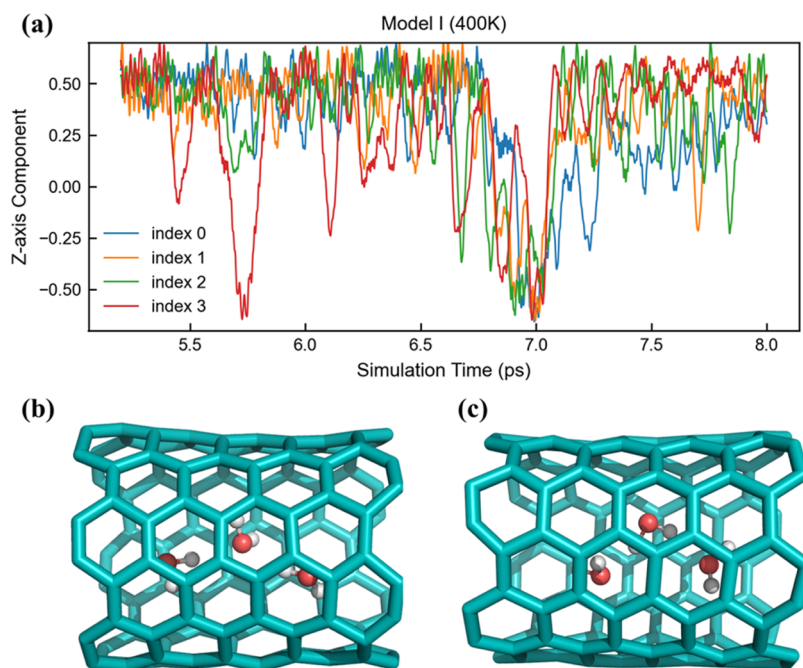
Figure 6. (a) Z-axis components of relative dipole moments of water molecules confined to the CNTs changes with simulation at 400 K in Case I. Indices 0, 1, 2, and 3 correspond to the water molecules distributed along the z-axis direction. (b) D defect at 400 K in Case I. (c) L defect at 500 K in Case I.

affecting essentially the analysis of the results. Therefore, the direction of the water dipole is opposite to the direction of the z-axis in Case II, and the z-axis components are minus. In addition, the large difference between the radial components and axial components of the dipole highlights the orientation of water molecules inside the CNTs. The water molecules are aligned approximately along the axial direction consistent with the jagged pattern of the O atoms' positions mentioned above. Figure S3 presents the average relative dipole moments of the water molecules inside the CNTs and the axial and radial components of the dipoles in Case I and Case II at different temperatures. It is observed that the total relative dipole moments are centered around 0.62 with small fluctuations and that the axial and radial components of the relative dipole moments fluctuate around 0.45 or −0.45 and 0.1 or −0.1, respectively, with larger fluctuations. Therefore, the narrow distribution of the total dipole moment also reflects the relative rigidity of the water molecules.

As shown in Figure S3a, the relative dipole moments of the water molecules in the CNTs with dangling bonds flip orientation at 400 and 500 K, while it does not occur at 300 K. It can also be seen in the corresponding statistical histogram in Figure 5a, in which there are some negative values about z-axis components of relative dipole moments at 400 and 500 K. Given that no external field is applied during the simulation, the flips here probably originate from the random thermal motion and the dangling bonds at the ends. Furthermore, when a water molecule inside the CNTs flips due to thermal motion and the interaction with the water molecules outside the tube, it can induce the dipole flip of other water molecules within the CNTs, so as to get lower energy. By examining the dipole flip process of water molecules, we find that the first water molecule achieving the dipole flip is basically located at the end of CNTs. In addition, when the water molecule located at the end flips, it does not necessarily mean that the other water molecules will also follow the flip, shown as in

Figure 6a. Perhaps the dipole flips of all water molecules inside the CNTs will be achieved only when certain conditions are met, such as the relative dipole moment of other water molecules deviates significantly from the axis due to thermal motion, which makes it easier to achieve the dipole flip with a lower energy barrier. It is worth noting that the duration of these dipole flip states is relatively short in the simulation at 400 K, at most about 1 ps. Later, the relative dipoles flip back to the original orientation. It is very different from the dipole flip duration of 2−3 ns mentioned in Hummer's study.[1] It is possible that due to the short duration of the simulation, the behavior with a longer characteristic time is not easily observed, and the above dipole flip is more likely to be a random, small-probability event. It can be inferred that the orientation of dipoles and their maintenance time is closely related to the water molecules' environment outside the CNTs. Nevertheless, just like Mukherjee et al. have proposed,[3] the dipole flips of all of the water molecules inside the CNTs are mediated by the hopping of D or L defects, two types of the orientational defects of hydrogen bonding, through the single-file water chain. In our simulations, the dipole flips are also accompanied by the D defect or L defect. Figure 6b,c shows the D defect at 400 K and L defect at 500 K in the simulation. These defects are not stable and only last for tens of femtoseconds. At 300 K no dipole flip occurs, and as a result, there is no defect in the simulation.

Figure S3b gives the relative dipole moment distributions of water molecules inside the CNTs of Case II. By contrast, these characteristics are similar to Case I, including the magnitude of relative dipole moments and the relationship between the axial components and radial components. However, there are some differences between Case I and Case II. First, since the relative dipole moment direction is opposite to the axial direction, the axial components of the relative dipole moment are negative as mentioned above. Next, the z-axis components of the dipole remain negative at 300 and 400 K, and the dipole flips only at
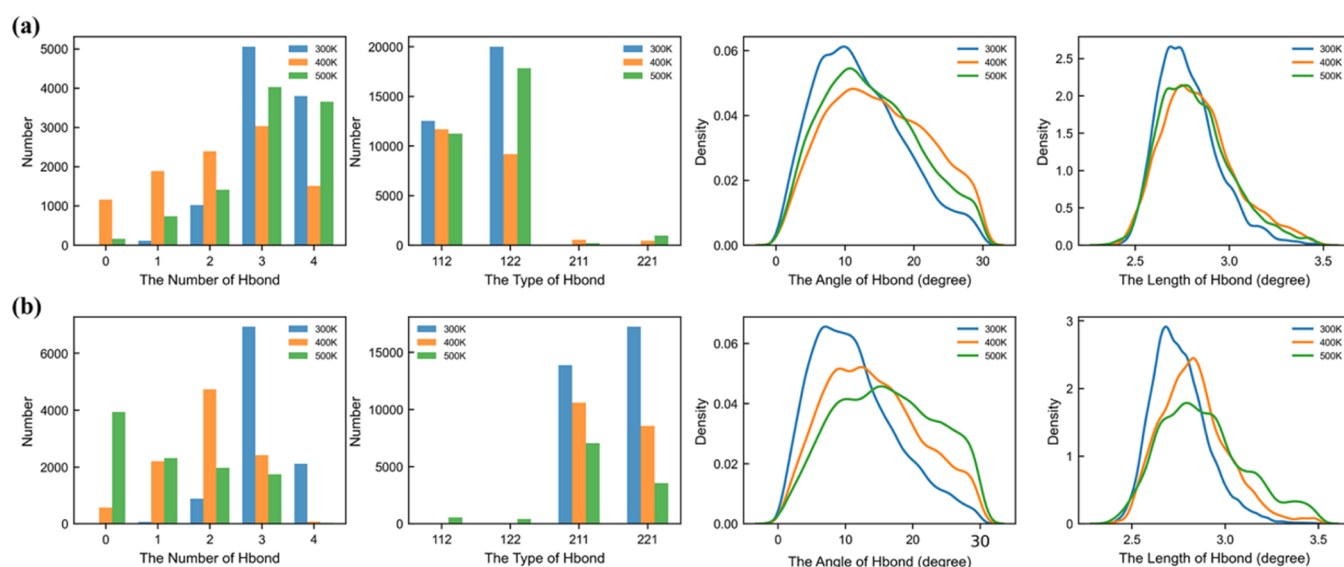
Figure 7. Analysis results of hydrogen bonds formed inside the CNTs of Case I (a) and Case II (b) at different temperatures (blue for 300 K, orange for 400 K, and green for 500 K). From left to right, the distributions of the number of hydrogen bonds, hydrogen bond types, hydrogen bond angles, and hydrogen bond lengths are plotted in this order.

500 K. In the meantime, in the simulation after 7 ps, the radial components do not maintain around 0.1 or −0.1. Instead, they fluctuate over a wide range. Actually, in this simulation process, there is only one water molecule inside the CNTs and the dipole gets easier to rotate and flip without the constraints of hydrogen bonding.

Hydrogen Bond Analysis. Consistent with earlier reports, our AIMD simulation indicates that water molecules inside narrow CNTs form a single file of hydrogen bonds. Figure 7 shows the analysis results of hydrogen bonds formed inside the CNTs of Case I and Case II at different temperatures, including the distribution of the hydrogen bonding number, type, angle, and bond length. The criteria for hydrogen bonding and the definition of hydrogen bond types have been presented in the Methods part. For Case I, a greater number of hydrogen bonds are formed at 300 K, followed by 500 K, and the least at 400 K, as shown in Figure 7a, which is consistent with the number of water molecules inside the CNTs analyzed above, as shown in Figure S1. Likewise, a similar situation exists for Case II. The bond angles and bond lengths of hydrogen bonds are on average around 14° and 2.8 Å, as shown in Figure 7a,b. In addition, the distribution of bond angles of hydrogen bonds approximately shows normality, with a little positive skewness. It is worth noting that for both Case I and Case II, the hydrogen bond angles and lengths are smaller at 300 K compared to both 400 and 500 K, which is relative to the number of hydrogen bonds or water molecules inside the CNTs as analyzed above.

Figure 7a,b also shows the statistical histogram of the types of all hydrogen bonds. For Case I, only "112" and "122" types exist at 300 K. But at 400 and 500 K, there are a large number of hydrogen bonds of "112" and "211" types, and a small number of "211" and "221" types. Actually, the latter corresponds to the dipole flip mentioned above at 400 and 500 K. When the dipole flips, the donor O and acceptor O swap roles. The hydrogen bond type "1*2" will change to type "2*1", and the change of the hydrogen bond type from "112" to "122" indicates the hydrogen bond angular jump mentioned below. Similarly, for Case II, the hydrogen bond types only

include "211" and "221" at 300 and 400 K, consistent with the fact that the dipole's direction is reversed to the axis. There are no changes from "2**" to "1**". By contrast, the shift exists at 500 K, which means that the dipole flip occurs only at 500 K in Case II. In a word, temperature and the presence of dangling bonds at the ends of CNTs are the factors that perturb the hydrogen-bonding network. When the temperature is lower and there are no dangling bonds at the ends of the CNTs, the water molecules inside the CNTs tend to form a more stable hydrogen-bonding network. The hydrogen bond is relatively strong with shorter bond lengths and smaller bond angles. Moreover, in the more stable hydrogen-bonding network, water molecules are less likely to flip over.

Hydrogen Bond Angular Jump. The angular jump refers to the exchange of H atoms in the donor of the hydrogen bond,[22] as shown in Figure 8. In our simulations of both Case I
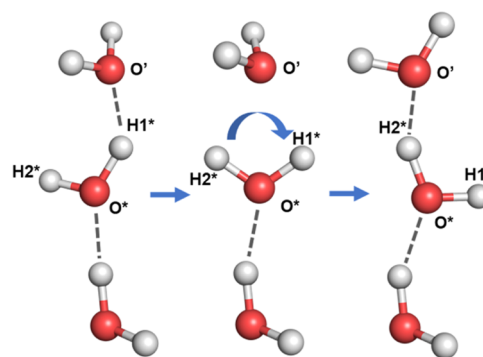

Figure 8. Hydrogen bond angular jump.

and Case II, there exist frequent hydrogen bond angle jumps among water molecules inside the CNTs at three temperatures. Figure S4 shows the variation of the hydrogen bonding type with simulation time for two selected water molecules adjacent to each other within the CNTs at three temperatures in Case I and Case II. For example, in Figure S4a corresponding to Case I, the hydrogen bond of these two water molecules presents
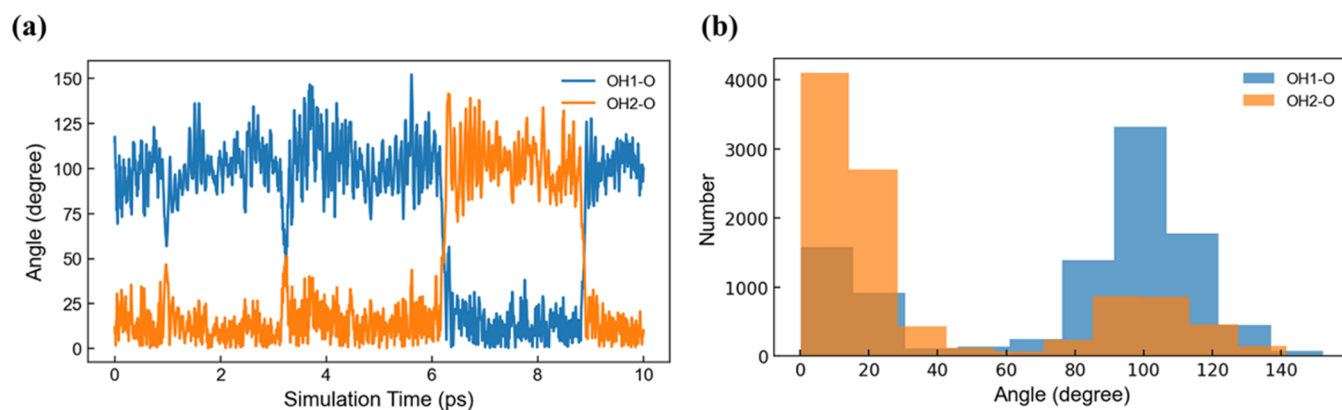
Figure 9. (a) Variation of the bond angle formed by the O atom (vertex) and H atom of one water molecule with the O atom of the neighboring water molecule inside the CNTs of Case I with the simulation time at 300 K. (b) Statistical distribution of the above angles.
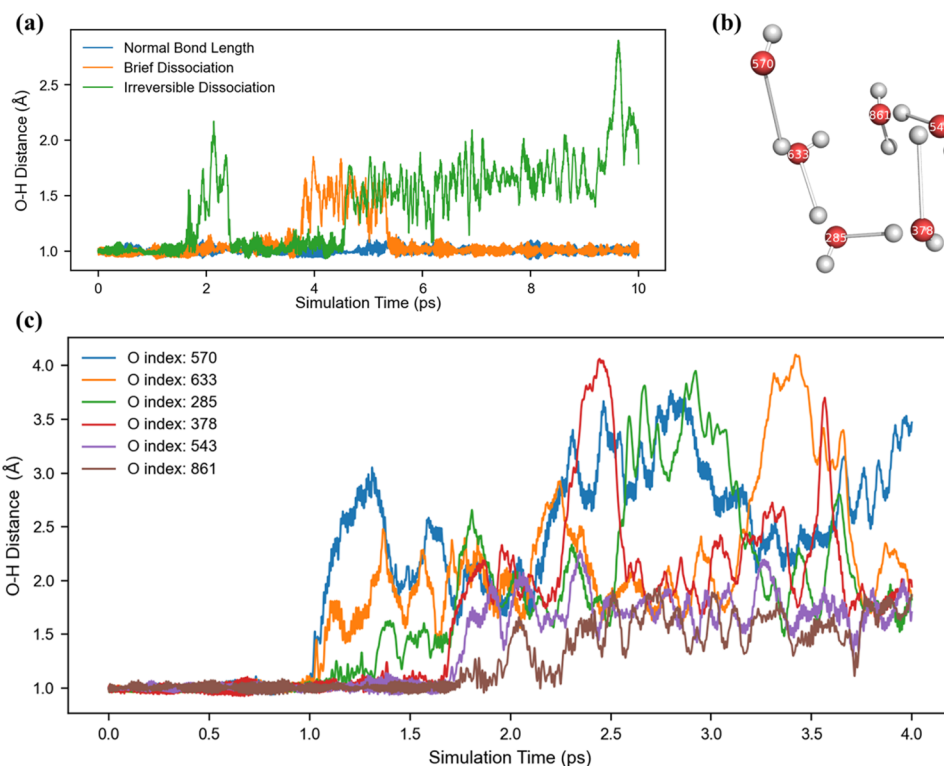

Figure 10. (a) Three scenarios for the variation of the O−H distance with simulation time. (b) Proton conduction among some water molecules aligns the hydrogen-bonding network. (c) Variation of the O−H distance of water molecules involved in the proton conduction with the simulation time.

three types at 300 K: "0", "112", and "122". Type "0" means that these two water molecules do not satisfy the condition for hydrogen bonding, while the shift of the hydrogen bond type "112" to "122" indicates the transition in the H atom attached to the donor O atom, which implies an angular jump in hydrogen bonding. At 400 and 500 K, again the angular jump in hydrogen bonding can be more frequently found in both Case I and Case II. In addition, the transition of the hydrogen bond type from "122" or "112" to "221" or "212" at 400 and 500 K in Case I is exactly the flip of the dipole mentioned above. It can be seen that the angular jump is more likely to occur than the dipole flips and the hydrogen bonding states are maintained for a longer period of time.

To characterize this angular jump more quantitatively, Figure 9a shows the variation of the bond angle formed by the

O atom (vertex) and H atom of one water molecule with the O atom of the neighboring water molecule inside the CNTs with the simulation time at 300 K in Case I. Figure 9b then gives the statistical distribution of these bond angles. These angles are basically distributed around 15 and 100°, showing bistability and corresponding to the position where the two H atoms are located. There are similar phenomena in Case II. Figure S5 shows the hydrogen bond angular jump at 300 K in Case II.

Dangling Bonds Promote the Dissociation of Water Molecules. In the AIMD simulations, it is examined by electronic structure calculations, i.e., the first principle is used to calculate the interaction forces among atoms. So different from the water molecules' model such as SPC, SPC/E, and TIP3P used in classical MD, AIMD simulation can be able to dynamically and more realistically simulate the conformational
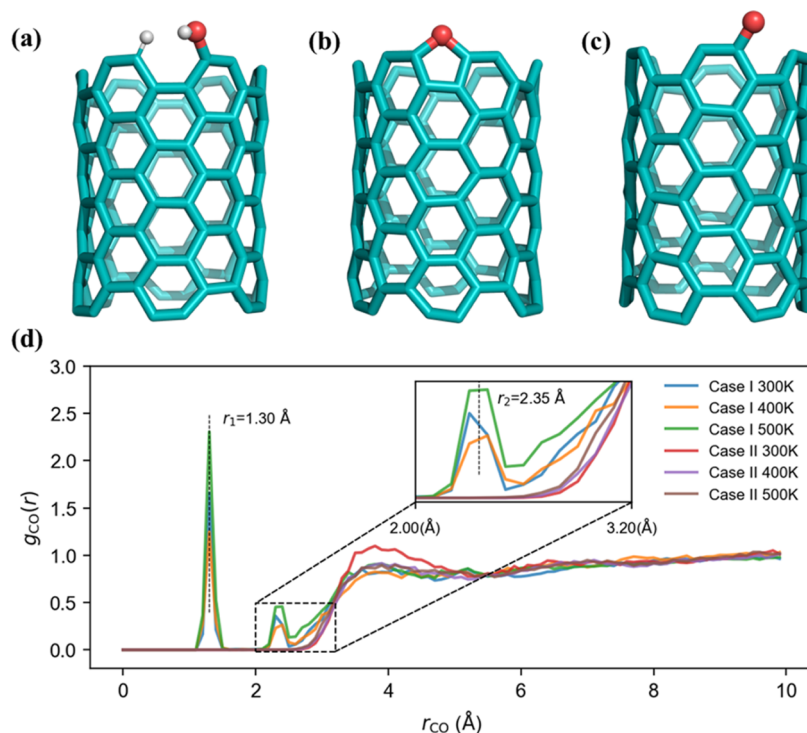
Figure 11. Dangling bonds capped by hydrogen and hydroxyl at 300 K (a), by the ether bond at 400 K (b), and by carbonyl at 500 K (c). (d) Radial distribution functions (RDF) of C atoms carrying dangling bonds and O atoms in Case I. The RDF of the C atom with the same locations as in Case I and the O atom in Case II.

changes of the water molecules. The bond angle and length of water molecules change with evolution and are not fixed. By examining the H atom and O atom of the water molecule, we find that the distance of both atoms of some water molecules far exceeds the reasonable bond length (0.96 Å) during the simulation, which means that the water molecules dissociate. In this work, if the distance of H and O atoms of the same water molecule is greater than 1.2 Å, we think the dissociation occurs, that is to say, 1.2 Å is the criteria for judging whether the water molecule dissociates. Specifically, we explore the changes in bond lengths of all of the water molecules with time and count the number of water molecules with an OH distance greater than a reasonable length. At 300, 400, and 500 K, 40, 39, and 43 water molecules dissociate, respectively, in Case I, accounting for 15.8, 15.4, and 17.0%, respectively. It can be observed that there are more water molecules dissociating at 500 K. However, the differences in the number of water molecules dissociated are not significant, which means that the impact of temperature does not manifest itself. In Case II, though the bond length of some water molecules exceeds the set criteria, that is, 1.2 Å, there is no irreversible dissociation, that is to say, the H atom and O atom still form the original water molecule, and the OH bond of these water molecules fluctuates over a wider range. Based on this, we demonstrate that the temperature independence is the result of dangling bonds at the ends of CNTs in Case I. Figure S6 presents the variation of bond lengths of five water molecules with a simulation time of Case II at three temperatures. These molecules are the top five water molecules in the simulation in terms of their maximum bond length. It is worth noting that there are only four water molecules whose bond lengths are greater than 1.2 Å for a shorter time at 300 K. In addition, there are only 17 and 25 water molecules with the bond length

exceeding 1.2 Å briefly at 400 and 500 K, respectively, much lower than those in Case I. These also indicate that it is the effects of dangling bonds that lead to the dissociation of water molecules in Case I. As for the differences in the number of short-time dissociation of water molecules in Case II, we think that these rather reflect the effect of temperature. Especially, the great increase between 300 and 400 K hints at the existence of the phase transition between them.

The following gives a more detailed description of the dissociation of water molecules in Case I. Figure 10a shows three scenarios for the variation of the O−H distance in Case I, which are, respectively, the normal bond length range, a brief dissociation but a subsequent return to normal, and irreversible dissociation. It is worth noting that the water molecules that appear to dissociate in the simulations at three temperatures are located outside the CNTs, and the O−H distances of the water molecules inside the CNTs are kept in the normal range. It is to be added that this is also true for Case II. Roughly speaking, there are only several water molecules inside the CNTs, and it is relatively easy to understand in terms of the magnitude of the probability of occurrence only.

Through further analysis, we observe that there exists a close connection between the water molecules whose O−H distance exceeds the set value during the simulation in Case I, and there actually exists proton conduction between them. Concretely, if water molecule A dissociates to form a proton and hydroxide ion, the proton will combine with the surrounding water molecule such as B in the direction of a hydrogen bond to form a hydrated proton. The hydrated proton will dissociate quickly to produce another proton and a water molecule, and the proton or hydrogen atom at this point is from water molecule B itself instead of A, which suggests that proton conduction is the hopping of hydrogen atoms of different

water molecules along the network of hydrogen bonds, and in the simulation, the whole process will involve several water molecules. Obviously, the way of proton conduction in the above is similar to the excess proton conduction in the aqueous system illustrated by the Grotthuss mechanism[31] that the proton can conduct along the hydrogen-bonding network in a hopping manner. Moreover, if we consider proton conduction with the hydrated proton as the starting point, we will find that the formation of a proton from a hydrogen atom away from the O atom causes the breakage of the hydrogen bond, in which the hydrated proton offers the donor O. The proton then binds to an O atom of another water molecule, and the formation of a new hydrated proton leads to the formation of a new hydrogen bond and it contributes to the donor O. This is a similar process that Agmon mentioned in the literature.[31] Fig-Figure 10b,c illustrates such a process in Case I at 300 K. The water molecule with index 570 first dissociates, and the consequently formed proton close to the next water molecule with index 663 prompts its dissociation. As just mentioned, the dissociation of one water molecule drives the dissociation of other water molecules through proton conduction. Next is the dissociation of the remaining water molecules, as shown in Figure 10b.

Overall, the dangling bonds at the ends of CNTs promote the dissociation of water molecules outside the CNTs. By comparing Case I and Case II, it can be found that the influence of dangling bonds is stronger than the influence of temperature. In Case II without dangling bonds, the effects of temperature can be observed. What both Case I and Case II have in common is that the water molecules with OH bond lengths longer than 1.2 Å are located outside the CNTs, and the results may be related to the suppression of the self-dissociation of water molecules by the one-dimensional confinement mentioned in this literature.[55] The possible reason is that in bulk water, protons or hydrated protons, and hydroxide ions formed by ionization of water molecules have abundant hydrogen-bonding networks or solvation shells to stabilize them. While inside the narrow CNTs, there are fewer hydrogen bonds and the distribution of the hydrogen bond is unique, which is not conducive to the formation of a solvation shell to stabilize hydrated protons and hydroxide ions. Therefore, the dissociation of water molecules inside the CNTs is suppressed.

Passivation of Dangling Bonds. In Case I, the dangling bonds promote the dissociation of water molecules, forming proton and hydroxide ions. Through examining the whole simulation process, we find that the C atoms with dangling bonds are very reactive and some bond with the H atom or hydroxyl group, that is, they are passivated. The passivation processes are observed in the simulations at different temperatures, and almost all appear very early, even at 1.05 ps at 300 K. Supporting Video 1 illustrates that one water molecule approaches the C atom carrying a dangling bond in the simulation process at 300 K, and in the process, the water molecule dissociates into the proton and hydroxide. Then, these two products are successively bonded to two C atoms, and the final result can be seen in Figure 11a. In fact, during the passivation process, the C atoms with dangling bonds are not only capped by the H atom and a hydroxyl group but also by the O atom to form the ether bond or the carbonyl group. Figure 11b,c shows the ether bond and carbonyl group formed by the passivation of the C atom with a dangling bond, respectively. It should be noted that the passivation by ether

bond only occurs at 400 K, and the passivation by carbonyl only occurs at 400 and 500 K in our simulations.

In Case I, there are 24 carbon atoms carrying dangling bonds. Maybe owing to the short simulation time, not all C atoms are passivated, even though there exist some protons or hydroxide ions at 10 ps. But by coincidence, exactly 10 of them are passivated at all different temperatures. These passivated C atoms, two by two, are adjacent and bonded to each other. Moreover, in these two adjacent passivated C atoms, one bonds to the O atom and the other bonds to the H atom. In our simulations, we find that the O atom approaches the C atom a bit earlier or almost simultaneously than the proton approaches the corresponding C atom, as shown in Figure S7, in which these two C atoms are adjacently bonded as mentioned above. More specific passivation results at 10 ps can be found in Supporting Videos 2−4 which correspond to 300, 400, and 500 K, respectively. Then, we calculate the radial distribution functions (RDF) of C−O. Specifically, we take these C atoms carrying dangling bonds in Case I as the central atom, examine the O atoms around them, and finally obtain the RDF. For Case II, we select the C atoms with the same locations as Case I. The RDFs at different temperatures in Cases I and II are shown in Figure 11d. It can be seen that there exist O atoms around the dangling bonds at $r_1 = 1.30$ Å and $r_2 = 2.35$ Å in Case I, which is significantly different from the situations in Case II. In combination with the passivation mentioned above, the first peak corresponds to the O atoms bonded with C atoms like the hydroxyl, ether bond, or carbonyl at $r_1 = 1.30$ Å, and the second peak at $r_2 = 2.35$ Å corresponds to the position relationship between O atoms and the neighboring C atoms of the passivated C atoms. So in general, compared with Case II, the passivated ends of CNTs in Case I are more hydrophilic than those in Case II, and to some extent, this can explain why the number of water molecules inside the CNTs in Case II is relatively low.

■ CONCLUSIONS

The structure and dynamic properties of water molecules inside the narrow CNTs are analyzed at different temperatures through AIMD simulation for two types of endings. Whether in Case I or Case II, it has been observed that water molecules confined to the CNTs manifest a jagged pattern and the hydrogen bond angular jump easily occurs in the simulation at different temperatures. Apart from this, the relative dipole moments of water molecules are approximately along the axis, and when the dipole flips, there are brief D defect or L defect states inside the CNTs in Case I. Furthermore, with the advantages of AIMD, we can observe the dissociation of water molecules and related proton conduction in Case I. During the simulation, the dissociating water molecules are all located outside the CNTs in both cases. Therefore, our simulations support the conclusion that one-dimensional CNTs suppress the dissociation of water molecules to some extent. In addition, as analyzed above, there are some differences between Case I and Case II. For Case II, the H atoms at the ends of CNTs with hydrophobicity and steric resistance inhibit water molecules from staying inside the CNTs or discourage the entry of water molecules from outside, especially at a higher temperature. These lead to fewer water molecules inside the CNTs in Case II. The number of water molecules within the CNTs influences the hydrogen-bonding network and, in turn, the movement of water molecules within the CNTs, including the orientation of the dipoles, bond lengths, and bond angles

of the hydrogen bonds. Conversely, the presence of dangling bonds in Case I promotes the dissociation of water molecules. The C atoms with dangling bonds at the ends of CNTs in Case I attract the water molecules outside the CNTs strongly, promoting the ionization of water molecules. Afterward, passivation processes take place in Case I. The C atoms with dangling bonds are capped with hydrogens, hydroxyl, ether bond, or carbonyl. In terms of water dissociation, the influence of dangling bonds is stronger than the effect of temperature and these water molecules dissociate in almost similar proportions at different temperatures in Case I.

Owing to the high cost of AIMD simulations, our simulations were only conducted for 10 ps, much smaller than the running time of classical MD. Therefore, we do not examine or observe related properties with long-time characteristics, such as the transport behaviors inside the CNTs and the overall relative dipole moments' flip. It is worth noting that the CNTs are not fixed during the simulations and their structure undergoes a smaller deformation, which may impact the dynamic properties of water molecules inside the CNTs. It deserves follow-up attention and research. In fact, it is common practice in classical MD to fix the CNTs. In the classical MD simulations, it is not possible to study the nature of the dangling bonds. In a word, this is the first study to simulate the CNTs centered in a water box with nearly 900 atoms using the AIMD method. The above findings will be helpful for studying the structure and dynamic properties of water molecules confined to narrow CNTs. In addition, it will help researchers to adopt more suitable methods based on the questions to be studied, such as whether the CNTs are fixed or not, whether the CNTs have dangling bonds at their ends, and whether to use MD or AIMD. At last, we believe this study will offer fresh insights into confinement effects, thermal fluctuation effects, and terminal effects of the CNTs and can be helpful for diverse technological applications.

ASSOCIATED CONTENT

Ⓢ Supporting Information

The Supporting Information is available free of charge at https://pubs.acs.org/doi/10.1021/acsomega.2c05588.

> Structure properties of water molecules inside the CNTs in Cases I and II (Figures S1–S5); variation of the O–H distance of these top five water molecules in the simulation in Case II (Figure S6); and the variation of C–O and C–H distances during the passivation processes in Case I (Figure S7) (PDF)
>
> One water molecule approaches the C atoms carrying a dangling bond from 0 to 7 ps in the simulation at 300 K and finally passivates the C atoms by hydrogen and hydroxyl (MP4)
>
> Final passivation effects, *i.e.*, at 10 ps in Case I at 300 K (MP4)
>
> Final passivation effects, *i.e.*, at 10 ps in Case I at 400 K (MP4)
>
> Final passivation effects, *i.e.*, at 10 ps in Case I at 500 K (MP4)

AUTHOR INFORMATION

Corresponding Author

Diannan Lu − *Department of Chemical Engineering, Tsinghua University, Beijing 100084, P. R. China;* ⓞ orcid.org/0000-0001-5993-5626; Email: ludiannan@tsinghua.edu.cn

Authors

Dongfei Liu − *Department of Chemical Engineering, Tsinghua University, Beijing 100084, P. R. China*

Jipeng Li − *School of Materials Science and Engineering, Hainan University, Haikou 570228, P. R. China*

Jianzhong Wu − *Department of Chemical and Environmental Engineering, University of California, Riverside, California 92521, United States;* ⓞ orcid.org/0000-0002-4582-5941

Complete contact information is available at:
https://pubs.acs.org/10.1021/acsomega.2c05588

Author Contributions

The manuscript was written through contributions of all authors. All authors have given their approval to the final version of the manuscript.

Notes

The authors declare no competing financial interest.

■ ACKNOWLEDGMENTS

■ REFERENCES

(1) Hummer, G.; Rasaiah, J. C.; Noworyta, J. P. Water Conduction through the Hydrophobic Channel of a Carbon Nanotube. *Nature* **2001**, *414*, 188−190.

(2) Koga, K.; Gao, G. T.; Tanaka, H.; Zeng, X. C. Formation of Ordered Ice Nanotubes inside Carbon Nanotubes. *Nature* **2001**, *412*, 802−805.

(3) Mukherjee, B.; Maiti, P. K.; Dasgupta, C.; Sood, A. K. Strongly Anisotropic Orientational Relaxation of Water Molecules in Narrow Carbon Nanotubes and Nanorings. *ACS Nano* **2008**, *2*, 1189−1196.

(4) Zhu, Z.; Wang, D.; Tian, Y.; Jiang, L. Ion/Molecule Transportation in Nanopores and Nanochannels: From Critical Principles to Diverse Functions. *J. Am. Chem. Soc.* **2019**, *141*, 8658−8669.

(5) Ihsanullah. Carbon Nanotube Membranes for Water Purification: Developments, Challenges, and Prospects for the Future. *Sep. Purif. Technol.* **2019**, *209*, 307−337.

(6) Thomas, M.; Corry, B. A Computational Assessment of the Permeability and Salt Rejection of Carbon Nanotube Membranes and Their Application to Water Desalination. *Philos. Trans. R. Soc., A* **2016**, *374*, No. 20150020.

(7) Goh, P. S.; Ismail, A. F. Graphene-Based Nanomaterial: The State-of-the-Art Material for Cutting Edge Desalination Technology. *Desalination* **2015**, *356*, 115−128.

(8) Farimani, A. B.; Min, K.; Aluru, N. R. DNA Base Detection Using a Single-Layer MoS $_2$. *ACS Nano* **2014**, *8*, 7914−7922.

(9) Vlassiouk, I.; Kozel, T. R.; Siwy, Z. S. Biosensing with Nanofluidic Diodes. *J. Am. Chem. Soc.* **2009**, *131*, 8211−8220.

(10) Macha, M.; Marion, S.; Nandigana, V. V. R.; Radenovic, A. 2D Materials as an Emerging Platform for Nanopore-Based Power Generation. *Nat. Rev. Mater.* **2019**, *4*, 588−605.

(11) Liu, F.; Wang, M.; Wang, X.; Wang, P.; Shen, W.; Ding, S.; Wang, Y. Fabrication and Application of Nanoporous Polymer Ion-Track Membranes. *Nanotechnology* **2019**, *30*, No. 052001.

(12) Kumar, H.; Dasgupta, C.; Maiti, P. K. Structure, Dynamics and Thermodynamics of Single-File Water under Confinement: Effects of Polarizability of Water Molecules. *RSC Adv.* **2015**, *5*, 1893−1901.

(13) Moskowitz, I.; Snyder, M. A.; Mittal, J. Water Transport through Functionalized Nanotubes with Tunable Hydrophobicity. *J. Chem. Phys.* **2014**, *141*, No. 18C532.

(14) Zhu, F.; Schulten, K. Water and Proton Conduction through Carbon Nanotubes as Models for Biological Channels. *Biophys. J.* **2003**, *85*, 236−244.

(15) García-Fandiño, R.; Sansom, M. S. P. Designing Biomimetic Pores Based on Carbon Nanotubes. *Proc. Natl. Acad. Sci. U.S.A.* **2012**, *109*, 6939−6944.

(16) Li, Y.; Li, Z.; Aydin, F.; Quan, J.; Chen, X.; Yao, Y.-C.; Zhan, C.; Chen, Y.; Pham, T. A.; Noy, A. Water-Ion Permselectivity of Narrow-Diameter Carbon Nanotubes. *Sci. Adv.* **2020**, *6*, No. eaba9966.

(17) Kalra, A.; Garde, S.; Hummer, G. Osmotic Water Transport through Carbon Nanotube Membranes. *Proc. Natl. Acad. Sci. U.S.A.* **2003**, *100*, 10175−10180.

(18) Majumder, M.; Chopra, N.; Andrews, R.; Hinds, B. J. Enhanced Flow in Carbon Nanotubes. *Nature* **2005**, *438*, No. 44.

(19) Liu, Y.; Wang, Q.; Zhang, L.; Wu, T. Dynamics and Density Profile of Water in Nanotubes as One-Dimensional Fluid. *Langmuir* **2005**, *21*, 12025−12030.

(20) Liu, Y.; Wang, Q.; Wu, T.; Zhang, L. Fluid Structure and Transport Properties of Water inside Carbon Nanotubes. *J. Chem. Phys.* **2005**, *123*, No. 234701.

(21) Thomas, J. A.; McGaughey, A. J. H. Water Flow in Carbon Nanotubes: Transition to Subcontinuum Transport. *Phys. Rev. Lett.* **2009**, *102*, No. 184502.

(22) Chakraborty, S.; Kumar, H.; Dasgupta, C.; Maiti, P. K. Confined Water: Structure, Dynamics, and Thermodynamics. *Acc. Chem. Res.* **2017**, *50*, 2139−2146.

(23) Cao, W.; Huang, L.; Ma, M.; Lu, L.; Lu, X. Water in Narrow Carbon Nanotubes: Roughness Promoted Diffusion Transition. *J. Phys. Chem. C* **2018**, *122*, 19124−19132.

(24) Sam, A.; Prasad, V.; Sathian, S. P. Water Flow in Carbon Nanotubes: The Role of Tube Chirality. *Phys. Chem. Chem. Phys.* **2019**, *21*, 6566−6573.

(25) Losey, J.; Kannam, S. K.; Todd, B. D.; Sadus, R. J. Flow of Water through Carbon Nanotubes Predicted by Different Atomistic Water Models. *J. Chem. Phys.* **2019**, *150*, No. 194501.

(26) Srivastava, A.; Hassan, J.; Homouz, D. Effect of Size and Temperature on Water Dynamics inside Carbon Nano-Tubes Studied by Molecular Dynamics Simulation. *Molecules* **2021**, *26*, No. 6175.

(27) Wang, Q.; Liu, L.; Liu, C.; Song, J.; Gao, X. Size Effect in Determining the Water Diffusion Rate in Carbon Nanotubes. *J. Mol. Liq.* **2021**, *334*, No. 116034.

(28) Mendonça, B. H. S.; Ternes, P.; Salcedo, E.; de Oliveira, A. B.; Barbosa, M. C. Water Diffusion in Carbon Nanotubes: Interplay between Confinement, Surface Deformation, and Temperature. *J. Chem. Phys.* **2020**, *153*, No. 244504.

(29) Brewer, M. L.; Schmitt, U. W.; Voth, G. A. The Formation and Dynamics of Proton Wires in Channel Environments. *Biophys. J.* **2001**, *80*, 1691−1702.

(30) Ma, X.; Li, C.; Martinson, A. B. F.; Voth, G. A. Water-Assisted Proton Transport in Confined Nanochannels. *J. Phys. Chem. C* **2020**, *124*, 16186−16201.

(31) Agmon, N. The Grotthuss Mechanism. *Chem. Phys. Lett.* **1995**, *244*, 456−462.

(32) Cao, Z.; Peng, Y.; Yan, T.; Li, S.; Li, A.; Voth, G. A. Mechanism of Fast Proton Transport along One-Dimensional Water Chains Confined in Carbon Nanotubes. *J. Am. Chem. Soc.* **2010**, *132*, 11395−11397.

(33) Berezhkovskii, A.; Hummer, G. Single-File Transport of Water Molecules through a Carbon Nanotube. *Phys. Rev. Lett.* **2002**, *89*, No. 064503.

(34) Falk, K.; Sedlmeier, F.; Joly, L.; Netz, R. R.; Bocquet, L. Molecular Origin of Fast Water Transport in Carbon Nanotube Membranes: Superlubricity versus Curvature Dependent Friction. *Nano Lett.* **2010**, *10*, 4067−4073.

(35) Holt, J. K.; Park, H. G.; Wang, Y.; Stadermann, M.; Artyukhin, A. B.; Grigoropoulos, C. P.; Noy, A.; Bakajin, O. Fast Mass Transport Through Sub-2-Nanometer Carbon Nanotubes. *Science* **2006**, *312*, 1034−1037.

(36) Lu, D. Accelerating Water Transport through a Charged SWCNTs: A Molecular Dynamics Simulation. *Phys. Chem. Chem. Phys.* **2013**, *15*, 14447−14457.

(37) Liu, Y.-C.; Shen, J.-W.; Gubbins, K. E.; Moore, J. D.; Wu, T.; Wang, Q. Diffusion Dynamics of Water Controlled by Topology of Potential Energy Surface inside Carbon Nanotubes. *Phys. Rev. B* **2008**, *77*, No. 125438.

(38) Berendsen, H. J. C.; Grigera, J. R.; Straatsma, T. P. The Missing Term in Effective Pair Potentials. *J. Phys. Chem. A* **1987**, *91*, 6269−6271.

(39) Mark, P.; Nilsson, L. Structure and Dynamics of the TIP3P, SPC, and SPC/E Water Models at 298 K. *J. Phys. Chem. A* **2001**, *105*, 9954−9960.

(40) Jorgensen, W. L.; Chandrasekhar, J.; Madura, J. D.; Impey, R. W.; Klein, M. L. Comparison of Simple Potential Functions for Simulating Liquid Water. *J. Chem. Phys.* **1983**, *79*, 926−935.

(41) Car, R.; Parrinello, M. Unified Approach for Molecular Dynamics and Density-Functional Theory. *Phys. Rev. Lett.* **1985**, *55*, 2471−2474.

(42) Kühne, T. D.; Iannuzzi, M.; Del Ben, M.; Rybkin, V. V.; Seewald, P.; Stein, F.; Laino, T.; Khaliullin, R. Z.; Schütt, O.; Schiffmann, F.; Golze, D.; Wilhelm, J.; Chulkov, S.; Bani-Hashemian, M. H.; Weber, V.; Borštnik, U.; Taillefumier, M.; Jakobovits, A. S.; Lazzaro, A.; Pabst, H.; Müller, T.; Schade, R.; Guidon, M.; Andermatt, S.; Holmberg, N.; Schenter, G. K.; Hehn, A.; Bussy, A.; Belleflamme, F.; Tabacchi, G.; Glöß, A.; Lass, M.; Bethune, I.; Mundy, C. J.; Plessl, C.; Watkins, M.; VandeVondele, J.; Krack, M.; Hutter, J. CP2K: An Electronic Structure and Molecular Dynamics Software Package - Quickstep: Efficient and Accurate Electronic Structure Calculations. *J. Chem. Phys.* **2020**, *152*, No. 194103.

(43) Mann, D. J.; Halls, M. D. Water Alignment and Proton Conduction inside Carbon Nanotubes. *Phys. Rev. Lett.* **2003**, *90*, No. 195503.

(44) Wang, L.; Zhao, J.; Li, F.; Fang, H.; Lu, J. P. First-Principles Study of Water Chains Encapsulated in Single-Walled Carbon Nanotube. *J. Phys. Chem. C* **2009**, *113*, 5368−5375.

(45) Thiemann, F. L.; Schran, C.; Rowe, P.; Müller, E. A.; Michaelides, A. Water Flow in Single-Wall Nanotubes: Oxygen Makes It Slip, Hydrogen Makes It Stick. *ACS Nano* **2022**, *16*, 10775−10782.

(46) Gravelle, S.; Joly, L.; Ybert, C.; Bocquet, L. Large Permeabilities of Hourglass Nanopores: From Hydrodynamics to Single File Transport. *J. Chem. Phys.* **2014**, *141*, No. 18C526.

(47) Pronk, S.; Páll, S.; Schulz, R.; Larsson, P.; Bjelkmar, P.; Apostolov, R.; Shirts, M. R.; Smith, J. C.; Kasson, P. M.; van der Spoel, D.; Hess, B.; Lindahl, E. GROMACS 4.5: A High-Throughput and Highly Parallel Open Source Molecular Simulation Toolkit. *Bioinformatics* **2013**, *29*, 845−854.

(48) Huang, W.; Lin, Z.; van Gunsteren, W. F. Validation of the GROMOS 54A7 Force Field with Respect to β-Peptide Folding. *J. Chem. Theory Comput.* **2011**, *7*, 1237−1243.

(49) VandeVondele, J.; Krack, M.; Mohamed, F.; Parrinello, M.; Chassaing, T.; Hutter, J. Quickstep: Fast and Accurate Density Functional Calculations Using a Mixed Gaussian and Plane Waves Approach. *Comput. Phys. Commun.* **2005**, *167*, 103−128.

(50) Perdew, J. P.; Burke, K.; Ernzerhof, M. Generalized Gradient Approximation Made Simple. *Phys. Rev. Lett.* **1996**, *77*, 3865−3868.

(51) Goedecker, S.; Teter, M.; Hutter, J. Separable Dual-Space Gaussian Pseudopotentials. *Phys. Rev. B* **1996**, *54*, 1703−1710.

(52) Iannuzzi, M.; Hutter, J. Inner-Shell Spectroscopy by the Gaussian and Augmented Plane Wave Method. *Phys. Chem. Chem. Phys.* **2007**, *9*, 1599.

(53) Grimme, S. Semiempirical GGA-type density functional constructed with a long-range dispersion correction. *J. Comput. Chem.* **2006**, *27*, 1787−1799.

(54) Chen, M.; Hack, J.; Iyer, A.; Lin, X.; Opila, R. L.Chemical and Electrical Passivation of Semiconductor Surfaces. In *Encyclopedia of Interfacial Chemistry*; Wandelt, K., Ed.; Elsevier: Oxford, 2018; pp 547−552.

(55) Sirkin, Y. A. P.; Hassanali, A.; Scherlis, D. A. One-Dimensional Confinement Inhibits Water Dissociation in Carbon Nanotubes. *J. Phys. Chem. Lett.* **2018**, *9*, 5029−5033.